Cyclic-Prefixed Single-Carrier Transmission with Reconfigurable Intelligent Surfaces

Qiang Li[†], Miaowen Wen[#], Ertugrul Basar[$],
George C. Alexandropoulos[•], Kyeong Jin Kim[∨], and H. Vincent Poor[⋆]
[†]College of Information Science and Technology, Jinan University, Guangzhou 510632, China
[#]School of Electronic and Information Engineering, South China University of Technology, Guangzhou 510640, China
[$]Department of Electrical and Electronics Engineering, Koç University, Istanbul 34450, Turkey
[•]Department of Informatics and Telecommunications, National and Kapodistrian University of Athens, Greece
[∨]Mitsubishi Electric Research Laboratories, Cambridge, MA 02139, USA
[⋆]Department of Electrical and Computer Engineering, Princeton University, Princeton, NJ 08544, USA
Email: qiangli@jnu.edu.cn, eemwwen@scut.edu.cn, ebasar@ku.edu.tr,
alexandg@di.uoa.gr, kkim@merl.com, poor@princeton.edu

***Abstract*— In this paper, a cyclic-prefixed single-carrier (CPSC) transmission scheme with phase shift keying (PSK) signaling is presented for broadband wireless communications systems empowered by a reconfigurable intelligent surface (RIS). In the proposed CPSC-RIS, the RIS is configured according to the transmitted PSK symbols such that different cyclically delayed versions of the incident signal are created by the RIS to achieve cyclic delay diversity. A practical and efficient channel estimator is developed for CPSC-RIS and the mean square error of the channel estimation is expressed in closed-form. We analyze the bit error rate (BER) performance of CPSC-RIS over frequency-selective Nakagami-m fading channels. An upper bound on the BER is derived by assuming maximum-likelihood detection. Our simulation results in terms of BER corroborate the performance analysis and the superiority of CPSC-RIS over the conventional CPSC without an RIS and orthogonal frequency division multiplexing with an RIS.**

I. Introduction

As an alternative to orthogonal frequency division multiplexing (OFDM), CPSC shares some OFDM advantages, such as low-complexity implementation, while avoiding several OFDM drawbacks, such as a high peak-to-average power ratio and high sensitivity to carrier frequency offsets [1]. Moreover, CPSC with a maximum-likelihood (ML) or minimum mean square error (MMSE) receiver is able to extract multipath diversity in frequency-selective fading channels for reasonably large values of block sizes and practical values of BER, while OFDM cannot harvest any multipath diversity even with the optimal ML receiver [2]. CPSC is a promising solution to broadband wireless communications, and has been included in the 3GPP Long Term Evolution standard for uplink transmission [1].

Rich multipath components, however, are required in the propagation environment for CPSC to achieve a significant gain in terms of BER. Unfortunately, this requirement may not be satisfied in general. Cyclic delay diversity (CDD) [3] is a simple yet effective technique to solve this problem. By transmitting the same signal from multiple antennas equipped in a single transmitter with different cyclic delays, a multiple-input channel is equivalently transformed to a single-input one with increasing multipath diversity and without altering the receiver structure. For CDD-CPSC, the zero-forcing (ZF) receiver fails to obtain any diversity gain, while the ML and MMSE receivers are able to pick up diversity gains under some conditions, as pure CPSC without CDD. To maximize the performance gain of applying CDD to CPSC systems, non-linear equalizers, such as the frequency-domain Turbo equalizer [4] and the block iterative generalized decision feedback equalizer [5], were developed. In cooperative CPSC systems, distributed CDD can be implemented via multiple single-antenna transmitters [6]. It is worth noting that all of the above-mentioned CDD transmission schemes are based on multiple local or distributed transmit antennas, each equipped with a radio frequency (RF) chain. This configuration obviously complicates the system implementation, expands the hardware cost, and increases the power consumption.

Recently, RIS-assisted transmission has emerged as an easy-to-implement, low-cost, and green communication technique [7], [8]. On an RIS, there are a large number of passive reflecting elements, each of which is able to reflect and exert adjustable amplitude-phase changes on incident signals. In this sense, the amplitude-phase responses of RISs and associated channels can be reconfigured intentionally to achieve different purposes. By exploiting this property, RISs have been applied to enhance the wireless communications in terms of energy efficiency [9], secrecy rate [10], error performance [11], etc. In particular, an RIS can be considered as an RF chain-free multi-antenna device [12]. Inspired by this observation, the authors in [13] and [14] designed RIS-based multiple-input multiple-output transmission schemes for spatial multiplexing and Alamouti space–time block coding, respectively. In contrast to the above-mentioned RIS-related works that focus on narrowband wireless communications over flat fading channels, the authors in [15]–[17] studied RIS-aided OFDM broadband wireless communications, in which the channel state information (CSI) is estimated in the frequency domain without multipath diversity gains.

To the best of our knowledge, CPSC transmission tech-

niques have not been investigated for RIS-aided broadband wireless communications. Moreover, there have not been any reports of time-domain channel estimation methods for RIS-aided broadband frequency-selective channels in the literature. The fact that an RIS acts as a multi-element reflector has also not been exploited to implement CDD as well. To fill these gaps, we design a CPSC transmission scheme with CDD and PSK signaling for RIS-empowered broadband wireless systems to harvest multipath diversity gains. An efficient pilot-aided channel estimator, which is able to estimate the equivalent channel in the time domain via one transmission block, is developed for CPSC-RIS. In this sense, CPSC-RIS provides a new framework of channel estimation for RIS-aided broadband communications systems. Both ML and ZF/MMSE detectors are designed for CPSC-RIS. We analyze the BER performance of CPSC-RIS over frequency-selective Nakagami-m fading channels. An upper bound on the BER of CPSC-RIS is derived in closed-form by assuming the ML detection without channel estimation errors. From the BER analysis, the diversity order of CPSC-RIS is characterized.

Notation: Column vectors and matrices are denoted by lowercase and uppercase boldface letters, respectively. Superscripts $(\cdot)^*$, $(\cdot)^T$, and $(\cdot)^H$ stand for conjugate, transpose, and Hermitian transpose, respectively. The $N \times N$ identity matrix is symbolized by $\mathbf{I}_{N\times N}$. $\mathbf{0}_{1\times N}$ denotes an all-zero matrix of size $1 \times N$. $\mathrm{diag}\{\cdot\}$ transforms a vector into a diagonal matrix. $\Re\{\cdot\}$ returns the real part of a complex number. $j = \sqrt{-1}$ is the imaginary unit. $\mathcal{CN}(\mu, \sigma^2)$ represents the complex Gaussian distribution with mean μ and variance σ^2. The probability of an event and the probability density function (PDF) of a random variable are denoted by $\Pr(\cdot)$ and $p(\cdot)$, respectively. $E\{\cdot\}$ and $Var\{\cdot\}$ denote expectation and variance, respectively. $\|\cdot\|$ stands for the Frobenius norm. $Q(\cdot)$, $\Gamma(\cdot)$, and $\lfloor\cdot\rfloor$ represent the Gaussian Q-function, Gamma function, and floor function, respectively. $\mathrm{rank}(\cdot)$ and $\mathrm{Tr}(\cdot)$ denote the rank and trace of a matrix, respectively. $\odot$ and $\star$ represent the Hadamard product and linear convolution, respectively. $\angle(\cdot)$ denotes the phase of a complex number and $\mathrm{cir}(\cdot)$ denotes right circulant operation.

II. System Model

A block diagram of the proposed CPSC-RIS system is illustrated in Fig. 1, where a CPSC transmitter communicates with a receiver over frequency-selective block fading channels with the aid of an RIS. Both the transmitter and the receiver are equipped with a single antenna, while the RIS that is connected to a controller consists of N_R reflecting elements. The RIS controller follows the instructions from the transmitter to adjust the reflection coefficients of the RIS. However, N_R is typically a large number, which results in high overhead/complexity for channel estimation and coefficient adjustment. Hence, we adopt the grouping method [15], i.e., the total of N_R reflecting elements are partitioned into R reflecting groups, each of which consists of $N_G = N_R/R$ adjacent elements sharing a common reflection coefficient.[1] Accordingly, the reflection coefficient for the r-th group of the RIS is expressed as $\phi_r = a_r \exp(j\theta_r)$, where a_r is the amplitude coefficient and θ_r is the phase shift with $r = 1, \ldots, R$. For all r, we set a_r to unity and take $\theta_r \in [0, 2\pi)$ from a discrete set Θ.

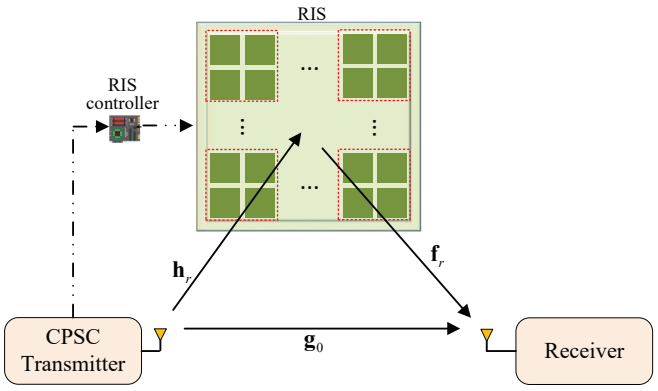


Fig. 1. The block diagram of the proposed CPSC-RIS system comprising a single-antenna transmitter, a multi-element RIS, and a single-antenna receiver.

The direct channel link from the transmitter to the receiver is described by the channel impulse response $\mathbf{g}_0 = [g_0(1), \ldots, g_0(L_0)]^T$, where L_0 is the number of channel taps for $\mathbf{g}_0$. The combined channels from the transmitter to the r-th reflecting group and from the r-th reflecting group to the receiver are denoted by $\mathbf{h}_r = [h_r(1), \ldots, h_r(L_{r0})]^T$ with L_{r0} channel taps and $\mathbf{f}_r = [f_r(1), \ldots, f_r(L_{r1})]^T$ with L_{r1} channel taps, respectively. The equivalent channel of the cascaded transmitter-RIS-receiver link associated with the r-th reflecting group is given by $\mathbf{g}_r = [g_r(1), \ldots, g_r(L_r)]^T = \mathbf{h}_r \star \mathbf{f}_r$ with $L_r = L_{r0} + L_{r1} - 1$. In this paper, the amplitude of $g_{\bar{r}}(l_{\bar{r}})$ is modeled as a Nakagami-m distribution with fading parameter $m_{\bar{r}}(l_{\bar{r}}) \in [1, 2, \ldots, \infty]$ and spreading parameter $\Omega_{\bar{r}}(l_{\bar{r}}) > 0$, i.e.,

$$p_{|g_{\bar{r}}(l_{\bar{r}})|}(x) = \frac{2m_{\bar{r}}(l_{\bar{r}})^{m_{\bar{r}}(l_{\bar{r}})} x^{2m_{\bar{r}}(l_{\bar{r}})-1}}{\Omega_{\bar{r}}(l_{\bar{r}})^{m_{\bar{r}}(l_{\bar{r}})}\Gamma(m_{\bar{r}}(l_{\bar{r}}))} \exp\left(-\frac{m_{\bar{r}}(l_{\bar{r}})x^2}{\Omega_{\bar{r}}(l_{\bar{r}})}\right),$$

where $\bar{r} = 0, 1, \ldots, R$ and $l_{\bar{r}} = 1, \ldots, L_{\bar{r}}$. The phase of $g_{\bar{r}}(l_{\bar{r}})$ is distributed uniformly over $[0, 2\pi)$ for all $\bar{r}$ and $l_{\bar{r}}$. Here, the channels associated with different reflecting groups are approximately considered as independent and identically distributed fading. We note that the practical case of correlated Nakagami-m fading [18], [19] will be considered in future work.

A. Transmitter Design

For each transmission, the CPSC transmitter modulates $b = N\log_2(M)$ information bits into a symbol vector $\mathbf{x} = [x(1), \ldots, x(N)]^T$, where $x(n)$ is a normalized M-ary PSK

[1] In practice, the grouping should be implemented according to the statistical characteristics of channels. The value of N_G can be obtained by trial and error for achieving a good trade-off between complexity, spectral efficiency, and error performance. Also, the number of reflecting elements in each group is not necessary to be equal.

symbol drawn from the constellation $\mathcal{X}$ for $n = 1, \ldots, N$. After adding an L-length CP to the beginning of $\mathbf{x}$, the transmitted data vector can be given by

$$\mathbf{x}_{CP} = [x(N-L+1), \ldots, x(N), x(1), \ldots, x(N)]^T, \quad (1)$$

where $L \geq \max\{L_0, \ldots, L_R\}$.[2] At this point, the transmitter derives the values of θ_r for all r based on $\mathbf{x}_{CP}$ and convey them to the RIS controller that further adjusts the R reflecting groups. It is worth noting that since $\mathbf{x}_{CP}$ is a PSK-modulated vector, cyclically delayed versions of $\mathbf{x}_{CP}$ can be constructed by performing phase shifts on $\mathbf{x}_{CP}$. To achieve CDD, θ_r is required to vary along with the transmission of $\mathbf{x}_{CP}$ and thus denoted by the vector $\boldsymbol{\theta}_r$ in the following. Moreover, by applying $\boldsymbol{\theta}_r$, the signal reflected from the r-th group of the RIS is expected to be a cyclically delayed version of $\mathbf{x}$, appended with an additional L-length CP, i.e.,

$$\mathbf{x}_{CP}(\Delta_r) = \Big[\underbrace{x(N-\Delta_r-L+1), \ldots, x(N-\Delta_r)}_{\text{CP}},$$
$$\underbrace{x(N-\Delta_r+1), \ldots, x(N), x(1), \ldots, x(N-\Delta_r)}_{\mathbf{x}(\Delta_r)}\Big]^T, \quad (2)$$

where $\mathbf{x}(\Delta_r)$ is the cyclically delayed version of $\mathbf{x}$ with the cyclic delay Δ_r for the r-th reflecting group. In CPSC-RIS, we let $\Delta_r = r\Delta$, where $L \leq \Delta \leq \lfloor N/(R+1) \rfloor$. From $\mathbf{x}_{CP} \odot \exp(j\boldsymbol{\theta}_r) = \mathbf{x}_{CP}(\Delta_r)$, for $r = 1, \ldots, R$, we have

$$\boldsymbol{\theta}_r = \Big[\angle x(N-\Delta_r-L+1) - \angle x(N-L+1), \ldots,$$
$$\angle x(N-\Delta_r) - \angle x(N), \ldots, \angle x(N-\Delta_r) - \angle x(N)\Big]^T \quad (3)$$

and $\Theta = \{0, 2\pi/M, \cdots, 2\pi(M-1)/M\}$.

At the receiver, after discarding the CP, the channel output is given by

$$\mathbf{y} = \mathbf{G}_0\mathbf{x} + \sum_{r=1}^{R} \mathbf{G}_r\mathbf{x}(\Delta_r) + \mathbf{w} = \sum_{\bar{r}=0}^{R} \mathbf{G}_{\bar{r}}\mathbf{x}(\Delta_{\bar{r}}) + \mathbf{w}, \quad (4)$$

where $\Delta_0 = 0$, $\mathbf{w} \in \mathbb{C}^{N\times 1}$ is the noise vector with the distribution $\mathcal{CN}(\mathbf{0}, N_0\mathbf{I}_{N\times N})$, and $\mathbf{G}_{\bar{r}}$ is an $N \times N$ circulant channel matrix given by $\mathbf{G}_{\bar{r}} = \text{cir}(\mathbf{g}_{\bar{r}}^0)$ with $\mathbf{g}_{\bar{r}}^0 = [\mathbf{g}_{\bar{r}}^T, \mathbf{0}_{1\times N-L_{\bar{r}}}]^T \in \mathbb{C}^{N\times 1}$. The signal-to-noise ratio (SNR) in this paper is defined as E_b/N_0 with $E_b = (N+L)/b$ being the average transmitted energy per bit. We can rewrite (4) as

$$\mathbf{y} = \sum_{\bar{r}=0}^{R} \mathbf{X}\mathbf{g}_{\bar{r}}^0(\Delta_{\bar{r}}) + \mathbf{w} = \mathbf{X}\mathbf{g}_{eq} + \mathbf{w}, \quad (5)$$

where $\mathbf{g}_{\bar{r}}^0(\Delta_{\bar{r}})$ is the cyclicly delayed version of $\mathbf{g}_{\bar{r}}^0$ with the cyclic delay $\Delta_{\bar{r}}$, $\mathbf{X}$ is an $N \times N$ circulant matrix represented by $\mathbf{X} = \text{cir}(\mathbf{x})$, and $\mathbf{g}_{eq}$ is given by

$$\mathbf{g}_{eq} = \sum_{\bar{r}=0}^{R} \mathbf{g}_{\bar{r}}^0(\Delta_{\bar{r}})$$
$$= [\mathbf{g}_0^T, \mathbf{0}_{1\times(\Delta-L_0)}, \mathbf{g}_1^T, \mathbf{0}_{1\times(\Delta-L_1)}, \ldots,$$
$$\mathbf{g}_R^T, \mathbf{0}_{1\times(N-R\Delta-L_R)}]^T.$$

We also define $\mathbf{g}'_{eq} = [g'_{eq}(1), \ldots, g'_{eq}(L_s)]^T = [\mathbf{g}_0^T, \mathbf{g}_1^T, \ldots, \mathbf{g}_R^T]^T$, which consists of $L_s = \sum_{\bar{r}=0}^{R} L_{\bar{r}}$ non-zero entries of $\mathbf{g}_{eq}$. As seen from (4) and (5), the cyclic delays on $\mathbf{x}$ are converted into those on channels. By denoting $\mathbf{G}_{eq} = \text{cir}(\mathbf{g}_{eq})$, (5) can be further expressed as

$$\mathbf{y} = \mathbf{G}_{eq}\mathbf{x} + \mathbf{w}. \quad (6)$$

B. Receiver Design

In this subsection, we successively design a pilot-aided channel estimator and various detectors for CPSC-RIS.

1) Channel Estimator: For channel estimation, a pilot vector $\mathbf{x}_p \in \mathbb{C}^{N\times 1}$, instead of a data vector $\mathbf{x}$, is transmitted from the CPSC transmitter, and the RIS is configured similarly to (3). Based on (5), the least-square estimation of $\mathbf{g}_{eq}$ is given by

$$\hat{\mathbf{g}}_{eq} = \mathbf{X}_p^{-1}\mathbf{y} = \mathbf{g}_{eq} + \mathbf{g}_e, \quad (7)$$

where $\mathbf{X}_p = \text{cir}(\mathbf{x}_p)$ and $\mathbf{g}_e = \mathbf{X}_p^{-1}\mathbf{w}$ represents the vector of channel estimation errors. $\mathbf{g}_e$ is independent of $\mathbf{g}_{eq}$ and follows the Gaussian distribution $\mathcal{CN}(\mathbf{0}, \sigma_e^2\mathbf{I}_{N\times N})$. The MSE of channel estimation can be derived as

$$\epsilon = E\{\|\mathbf{g}_e\|^2\} = \text{Tr}\left\{\mathbf{X}_p^{-1}E\{\mathbf{w}\mathbf{w}^H\}\left(\mathbf{X}_p^{-1}\right)^H\right\}$$
$$= N_0\text{Tr}\left\{\left(\mathbf{X}_p^H\mathbf{X}_p\right)^{-1}\right\}. \quad (8)$$

We observe from (8) that to minimize the MSE, $\mathbf{X}_p$ should satisfy $\mathbf{X}_p^H\mathbf{X}_p = N\mathbf{I}_{N\times N}$. In particular, using Zadoff-Chu sequences [20] as $\mathbf{x}_p$ meets this requirement. For N being an even number, we take $\mathbf{x}_p = [1, \exp(j\varpi\pi/N), \exp(j4\varpi\pi/N), \ldots, \exp(j\varpi\pi(N-1)^2/N)]^T$, where ϖ is an arbitrary integer relatively prime to N. Obviously, in this case, the achieved MSE is given by $\epsilon = N_0$ and we have $\sigma_e^2 = N_0/N$.

As described above, the channel estimation of CPSC-RIS can be completed via a single block of pilots regardless of the value of R. This is much faster than existing frequency-domain channel estimation methods for RIS-aided broadband communications systems, such as the one in [16] that requires $R+1$ transmission blocks to extract the CSI. With CSI, various detectors can be developed to recover $\mathbf{x}$, which will be described in the following.

2) ML Detector: From (5), the ML detector with the perfect CSI can be formulated as

$$\hat{\mathbf{x}} = \arg\min_{\mathbf{x}} \|\mathbf{y} - \mathbf{G}_{eq}\mathbf{x}\|^2, \quad (9)$$

where $\hat{\mathbf{x}} = [\hat{x}(1), \ldots, \hat{x}(N)]^T$ is the estimate of $\mathbf{x}$. Since the ML detector makes a joint decision on the N M-ary PSK symbols, the computational complexity in terms of complex multiplications is of order $\sim \mathcal{O}(M^N)$, which poses intolerable computational burden to the receiver. Thus, a low-complexity detector is highly recommended.

[2]The values of $L_0, \ldots, L_R$ are assumed to be known by using channel sounding schemes [6].

3) ZF/MMSE Detectors: Since $\mathbf{G}_{eq}$ is a circulant matrix, it has eigen decomposition $\mathbf{G}_{eq} = \mathbf{F}^H \mathbf{\Lambda} \mathbf{F}$, where $\mathbf{F}$ is the unitary discrete Fourier transform (DFT) matrix with $\mathbf{F}^H\mathbf{F} = \mathbf{I}_{N\times N}$, and $\mathbf{\Lambda}$ is the diagonal matrix whose diagonal elements are the N-point (non-unitary) DFT of $\mathbf{g}_{eq}$, i.e.,

$$\lambda(k) = \sum_{n=1}^{N} g_{eq}(n) \exp\left(-j\frac{2\pi(n-1)(k-1)}{N}\right), \quad (10)$$

where $k = 1, \ldots, N$. Therefore, based on (6), the frequency-domain received signal can be written as

$$\mathbf{y}_F = [y_F(1), \ldots, y_F(N)]^T = \mathbf{F}\mathbf{y} = \mathbf{\Lambda}\mathbf{x}_F + \mathbf{w}_F, \quad (11)$$

where $\mathbf{x}_F$ and $\mathbf{w}_F$ are the frequency-domain counterparts of $\mathbf{x}$ and $\mathbf{w}$, respectively. For frequency-domain ZF/MMSE equalization, $\mathbf{y}_F$ is fed into N single-tap equalizers in parallel, each of which is simply realized by one complex-valued multiplication, i.e.,

$$\hat{x}_F(n) = \phi(n) y_F(n), \quad n = 1, \ldots, N \quad (12)$$

where $\hat{x}_F(n)$ is the output of the n-th equalizer, and $\phi(n) = \lambda(n)^*/(|\lambda(n)|^2 + cN_0)$ with $c = 1$ for MMSE equalizer and $c = 0$ for ZF equalizer. Finally, we arrive at the estimated time-domain symbol vector via

$$\hat{\mathbf{x}} = \mathbf{F}^H \hat{\mathbf{x}}_F, \quad (13)$$

where $\hat{\mathbf{x}}_F = [\hat{x}_F(1), \ldots, \hat{x}_F(N)]^T$. Obviously, by using the single-tap equalization and the existing efficient algorithms for the implementation of DFT, the ZF/MMSE detectors achieve much lower computational complexity than the ML detector expressed by (9).

III. Performance Analysis

In this section, an upper bound on the BER of CPSC-RIS in the absence of channel estimation errors is provided after deriving the pairwise error probability (PEP) in closed-form.

Let us first study the conditional PEP, namely $\Pr(\mathbf{X} \to \hat{\mathbf{X}}|\mathbf{g}_{eq})$, which is the probability of detecting $\mathbf{X}$ as $\hat{\mathbf{X}}$ conditioned on $\mathbf{g}_{eq}$. From (5), (6), and (9), we have

$$\begin{aligned}\Pr\left(\mathbf{X} \to \hat{\mathbf{X}}|\mathbf{g}_{eq}\right) &= \Pr\left(\|\mathbf{y} - \mathbf{X}\mathbf{g}_{eq}\|^2 > \left\|\mathbf{y} - \hat{\mathbf{X}}\mathbf{g}_{eq}\right\|^2\right) \\ &= \Pr\left(V > 0\right), \end{aligned} \quad (14)$$

where $V = -\|(\mathbf{X} - \hat{\mathbf{X}})\mathbf{g}_{eq}\|^2 - 2\Re\{\bar{\mathbf{w}}^H(\mathbf{X} - \hat{\mathbf{X}})\mathbf{g}_{eq}\}$. We observe that V is Gaussian distributed with

$$\begin{aligned} E\{V\} &= -\left\|\left(\mathbf{X} - \hat{\mathbf{X}}\right)\hat{\mathbf{g}}_{eq}\right\|^2, \\ Var\{V\} &= 2N_0\left\|\left(\mathbf{X} - \hat{\mathbf{X}}\right)\hat{\mathbf{g}}_{eq}\right\|^2. \end{aligned}$$

Therefore, (14) can be calculated as

$$\Pr\left(\mathbf{X} \to \hat{\mathbf{X}}|\mathbf{g}_{eq}\right) = Q\left(\sqrt{\frac{\left\|\left(\mathbf{X} - \hat{\mathbf{X}}\right)\mathbf{g}_{eq}\right\|^2}{2N_0}}\right). \quad (15)$$

The squared norm $\|(\mathbf{X} - \hat{\mathbf{X}})\mathbf{g}_{eq}\|^2$ can equivalently be developed as

$$\begin{aligned}\left\|(\mathbf{X} - \hat{\mathbf{X}})_{[L_s]}\mathbf{g}'_{eq}\right\|^2 &= \mathbf{g}'^H_{eq}\mathbf{A}\mathbf{g}'_{eq} = \mathbf{g}'^H_{eq}\mathbf{U}^H\mathbf{D}\mathbf{U}\mathbf{g}'_{eq} \\ &= \sum_{l=1}^{L_s} d(l)|\tilde{g}_{eq}(l)|^2, \end{aligned} \quad (16)$$

where $(\mathbf{X} - \hat{\mathbf{X}})_{[L_s]}$ comprises L_s columns of $(\mathbf{X} - \hat{\mathbf{X}})$ corresponding to L_s non-zero entries of $\mathbf{g}_{eq}$, $\mathbf{A} = (\mathbf{X} - \hat{\mathbf{X}})^H_{[L_s]}(\mathbf{X} - \hat{\mathbf{X}})_{[L_s]}$ is decomposed as $\mathbf{A} = \mathbf{U}^H\mathbf{D}\mathbf{U}$ with $\mathbf{U}$ being a unitary matrix and $\mathbf{D} = \mathrm{diag}\{d(1), \ldots, d(L_s)\}$, and $\tilde{\mathbf{g}}_{eq} = [\tilde{g}_{eq}(1), \ldots, \tilde{g}_{eq}(L_s)]^T = \mathbf{U}\mathbf{g}'_{eq}$. Hence, (15) can be rewritten as

$$\Pr\left(\mathbf{X} \to \hat{\mathbf{X}}|\mathbf{g}_{eq}\right) = Q\left(\sqrt{\sum_{l=1}^{L_s} d(l)|\tilde{g}_{eq}(l)|^2/(2N_0)}\right).$$

Since $\tilde{g}_{eq}(l)$ is a linear combination of L_s entries of $\mathbf{g}'_{eq}$ with L_s tending to a large number, $\tilde{g}_{eq}(l)$ can be approximately modeled as a Gaussian random variable, i.e., $\tilde{g}_{eq}(l) \sim \mathcal{CN}(0, \sum_{l'=1}^{L_s}|u_{ll'}|^2\Omega_{l'})$, where $l = 1, \ldots, L_s$, $u_{ll'}$ is the (l, l')-th element of $\mathbf{U}$, and $\Omega_{l'}$ is the spreading parameter of $|g'_{eq}(l')|$, i.e., the l'-th entry of $[\Omega_0(1), \ldots, \Omega_0(L_0), \Omega_1(1), \ldots, \Omega_R(L_R)]^T$. We observe that $|\tilde{g}_{eq}(l)|^2$ is a central chi-square random variable, whose moment generating function is given by

$$\mathcal{M}(t) = \frac{1}{1 - t\sum_{l'=1}^{L_s}|u_{ll'}|^2\Omega_{l'}}. \quad (17)$$

Therefore, by using the well-known approximation $Q(x) \approx 1/12 \cdot e^{-x^2/2} + 1/4 \cdot e^{-2x^2/3}$, the unconditional PEP can be derived as (18), which is shown at the top of the next page. Finally, according to the union bounding technique, the BER of CPSC-RIS can be upper bounded by

$$P_e \leq \frac{1}{b2^b}\sum_{\mathbf{X}}\sum_{\hat{\mathbf{X}}}\Pr\left(\mathbf{X} \to \hat{\mathbf{X}}\right)\xi\left(\mathbf{X}, \hat{\mathbf{X}}\right), \quad (19)$$

where $\xi(\mathbf{X}, \hat{\mathbf{X}})$ is the number of erroneous bits when $\mathbf{X}$ is detected as $\hat{\mathbf{X}}$.

Remark: The contribution of L_s independent modified channel taps of $\tilde{\mathbf{g}}_{eq}$ to the unconditional PEP in (18) suggests that the highest possible diversity order is equal to L_s. However, this maximum diversity order is achieved if and only if $d(l)$ are non-null for all l, $\mathbf{X}$, and $\hat{\mathbf{X}}$. In general, the diversity order achieved by CPSC-RIS is given by $\min \mathrm{rank}(\mathbf{A})$. Since there exist some error events, such as $\mathbf{X} = \mathrm{cir}([1, \ldots, 1]^T)$ and $\hat{\mathbf{X}} = \mathrm{cir}([-1, \ldots, -1]^T)$, which make $\mathrm{rank}(\mathbf{A}) = 1$, the asymptotical (i.e., at infinite SNR) diversity order of CPSC-RIS is equal to one. Since this type of error events rarely occurs, simulation results in Section IV will show that the multipath diversity can be extracted by CPSC-RIS for moderate BER values and reasonably large values of N.

$$\Pr\left(\mathbf{X}\to\hat{\mathbf{X}}\right)\approx E\left\{\frac{1}{12}\prod_{l=1}^{L_s}\exp\left(-\frac{d(l)|\tilde{g}_{eq}(l)|^2}{4N_0}\right)+\frac{1}{4}\prod_{l=1}^{L_s}\exp\left(-\frac{d(l)|\tilde{g}_{eq}(l)|^2}{3N_0}\right)\right\}$$
$$=\frac{1}{12}\prod_{l=1}^{L_s}\left(1+\frac{d(l)}{4N_0}\sum_{l'=1}^{L_s}|u_{ll'}|^2\Omega_{l'}\right)^{-1}+\frac{1}{4}\prod_{l=1}^{L_s}\left(1+\frac{d(l)}{3N_0}\sum_{l'=1}^{L_s}|u_{ll'}|^2\Omega_{l'}\right)^{-1}. \quad (18)$$

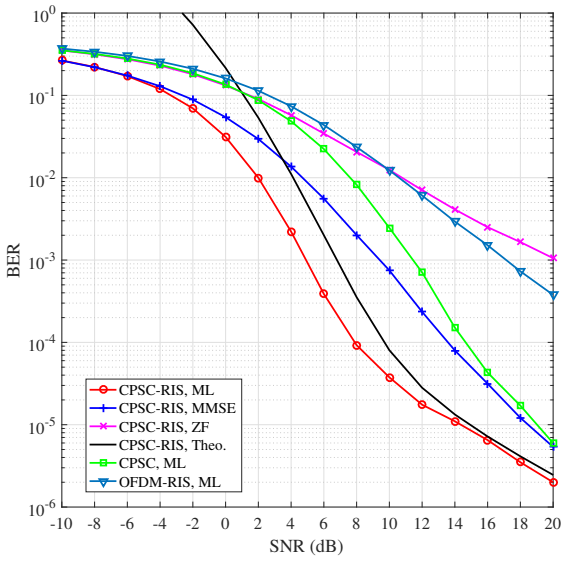


Fig. 2. Performance comparison among CPSC-RIS, CPSC, and OFDM-RIS, where $N=8, M=2, R=2$, and perfect CSI is assumed at the receiver.

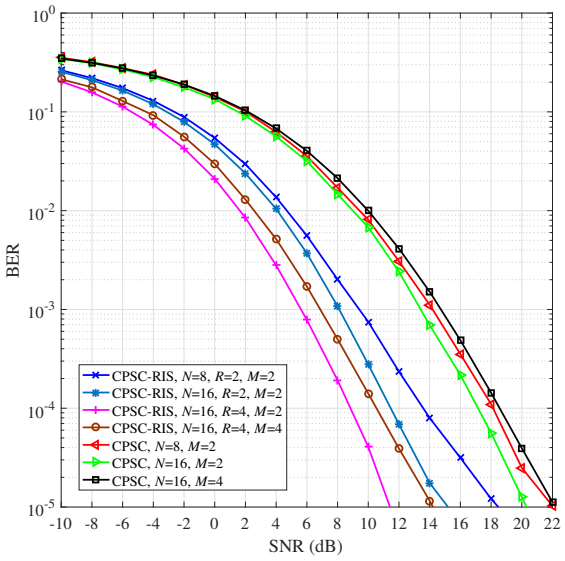


Fig. 3. Performance comparison between CPSC-RIS and CPSC, where $N=8,16, M=2,4, R=2,4$, and perfect CSI is assumed at the receiver.

IV. Simulation Results

In this section, we conduct Monte Carlo simulations to evaluate the uncoded BER performance of CPSC-RIS by taking CPSC and OFDM-RIS [16] as benchmarks. In OFDM-RIS, the RIS is configured to maximize the channel gain according to the method in [16] by assuming perfect CSI. In all simulations, we plot the BER versus SNR = E_b/N_0, and neglect any path loss effect of the channels that have a uniform power delay profile. For simplicity, we assume that $L_0=\cdots=L_R=2$, $m_0(1)=\cdots=m_0(L_0)=m_1(1)=\cdots=m_1(L_1)=\cdots=m_R(L_R)=2$, and $\Delta=L$.

Fig. 2 depicts the performance comparison among CPSC-RIS, CPSC, and OFDM-RIS, where $N=8, M=2, R=2$, and perfect CSI is assumed at the receiver. CPSC-RIS employs the ML, MMSE, and ZF detectors, while CPSC and OFDM-RIS use the ML detectors. To verify the analysis given in Section III, we also plot the BER upper bound (19) as a theoretical bound for the ML detector of CPSC-RIS in Fig. 2. As seen from Fig. 2, for CPSC-RIS with the optimal ML detection, the BER upper bound agrees with the simulation results in the high SNR region. In particular, for CPSC-RIS, the ZF detector cannot harvest any diversity and performs the worst. In contrast, for CPSC-RIS, both the ML and MMSE detectors achieve some diversity gains for practical BER values, while they fails to extract diversity gains at infinite SNR. Moreover, CPSC-RIS even with the low-complexity MMSE detector significantly outperforms conventional CPSC and OFDM-RIS with the optimal ML detectors throughout the considered SNR region. CPSC-RIS with the ML and MMSE detectors obtain approximately 7 dB and 1 dB SNR gains, respectively, over CPSC with the ML detector, at a BER value of 10^{-4}. Since the MMSE detector is able to achieve acceptable performance with the low implementation complexity, the MMSE detector is adopted for CPSC-RIS and CPSC in the rest of computer simulations.

Fig. 3 evaluates the BER performance of CPSC-RIS and CPSC, where $N=8,16, M=2,4, R=2,4$, and perfect CSI is assumed at the receiver. It can be observed from Fig. 3 that all considered CPSC-RIS schemes perform better than all CPSC schemes for all SNR values thanks to the extra R reflecting links introduced by the RIS, and the gain is more prominent for a larger value of R. For $N=16$ and $M=2$, CPSC-RIS with $R=4$ obtains about 3 dB SNR gain over that with $R=2$, at a BER value of 10^{-4}. Increasing the value of N achieves SNR gains of 2 dB and 1 dB for CPSC-RIS and CPSC, respectively, at a BER value of 10^{-4}. By contrast, a larger constellation size deteriorates the performance (about 2 dB SNR loss) for both CPSC-RIS and CPSC.

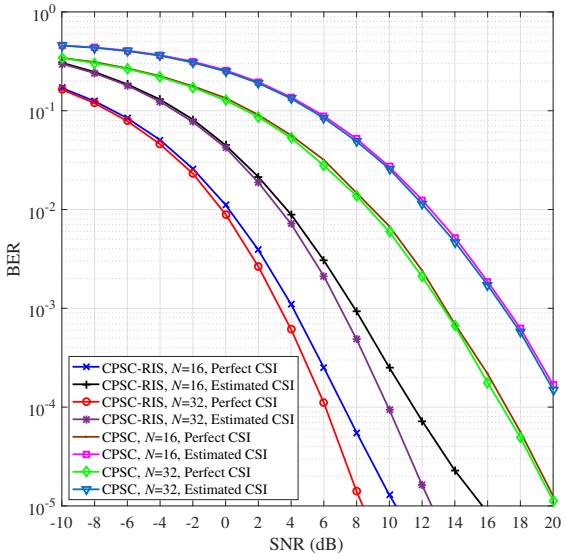


Fig. 4. Performance comparison between CPSC-RIS and CPSC, where $N = 16, 32$, $M = 2$, and $R = 6$. The cases of perfect channel estimation and practical channel estimation in (7) are considered.

Fig. 4 presents the performance comparison between CPSC-RIS and CPSC with perfect and estimated CSI at the receiver, where $N = 16, 32$, $M = 2$, and $R = 6$. The estimated CSI is obtained via (7). As expected, all schemes with estimated CSI perform worse than the corresponding schemes with perfect CSI, and approximately 4 dB SNR loss is incurred by the imperfect CSI. We observe from Fig. 4 that, in both cases, increasing the value of N from 16 to 32 leads to SNR gains for both CPSC-RIS and CPSC. Specifically, the SNR gain for CPSC-RIS is about 1 dB at a BER value of 10^{-4}, while that for CPSC is minor. With both perfect and estimated CSI at the receiver, CPSC-RIS outperforms CPSC for all considered SNR values. Moreover, for $N = 16$ and 32, CPSC-RIS with estimated CSI achieves about 6 dB and 7 dB SNR gains, respectively, over CPSC with perfect CSI, at a BER value of 10^{-4}.

V. Conclusion

In this paper, we have proposed a CDD-enhancing CPSC transmission scheme for RIS-aided broadband wireless systems. The channel estimation and signal detection have been studied for CPSC-RIS. Specifically, a practical and efficient time-domain channel estimator has been developed for CPSC-RIS, which can be considered as a general channel estimator for RIS-aided broadband communications. The optimal ML and low-complexity ZF/MMSE detectors have been designed for CPSC-RIS, and the BER performance of the ML detector over frequency-selective Nakagami-m fading channels has been analyzed with the theoretically derived upper bound.

Acknowledgment

This work was supported in part by the projects: National Natural Science Foundation of China under Grant 61871190, Guangdong Basic and Applied Basic Research Project under Grant 2021B1515120067, Natural Science Foundation of Guangdong Province under Grant 2018B030306005 and Grant 2020A1515110470, Chinese Postdoctoral Science Foundation under Grant 2021M691250, Scientific and Technological Research Council of Turkey (TUBITAK) under Grant 120E401, and EU H2020 RISE-6G project under Grant 101017011.

References

[1] F. Pancaldi *et al*., "Single-carrier frequency domain equalization," *IEEE Signal Process. Mag.*, vol. 25, no. 5, pp. 37–56, Sep. 2008.

[2] B. Devillers, J. Louveaux, and L. Vandendorpe. "About the diversity in cyclic prefixed single-carrier systems," *Physical Commun.*, vol. 1, no. 4, pp. 266–276, 2008.

[3] A. Dammann and S. Kaiser, "Standard comformable antenna diversity techniques for OFDM and its application to the DVB-T system," in *Proc. IEEE GLOBECOM*, San Antonio, TX, USA, Nov. 2001, pp. 388–397.

[4] U.-K. Kwon and G.-H. Im, "Cyclic delay diversity with frequency domain turbo equalization for uplink fast fading channels," *IEEE Commun. Lett.*, vol. 13, no. 3, pp. 184–186, Mar. 2009.

[5] Y. Liang, W. S. Leon, Y. Zeng, and C. Xu, "Design of cyclic delay diversity for single carrier cyclic prefix (SCCP) transmissions with block-iterative GDFE (BI-GDFE) receiver," *IEEE Trans. Wireless Commun.*, vol. 7, no. 2, pp. 677–684, Feb. 2008.

[6] K. J. Kim *et al*., "Performance analysis of distributed single carrier systems with distributed cyclic delay diversity," *IEEE Trans. Commun.*, vol. 65, no. 12, pp. 5514–5528, Dec. 2017.

[7] E. Basar *et al*., "Wireless communications through reconfigurable intelligent surfaces," *IEEE Access*, vol. 7, pp. 116753–116773, 2019.

[8] M. Di Renzo *et al*., "Smart radio environments empowered by AI reconfigurable meta-surfaces: An idea whose time has come," *EURASIP J. Wireless Commun. Netw.*, 129, pp. 1–20, May 2019.

[9] C. Huang *et al*., "Reconfigurable intelligent surfaces for energy efficiency in wireless communication," *IEEE Trans. Wireless Commun.*, vol. 18, no. 8, pp. 4157–4170, Aug. 2019.

[10] G. C. Alexandropoulos, K. Katsanos, M. Wen, and D. B. da Costa, "Safeguarding MIMO communications with reconfigurable metasurfaces and artificial noise," in *Proc. IEEE ICC*, Montreal, Canada, Jun. 2021, pp. 1–6.

[11] J. Ye, S. Guo, and M.-S. Alouini, "Joint reflecting and precoding designs for SER minimization in reconfigurable intelligent surfaces assisted MIMO systems," *IEEE Trans. Wireless Commun.*, vol. 19, no. 8, pp. 5561–5574, Aug. 2020.

[12] E. Calvanese Strinati, G. C. Alexandropoulos *et al*., "Reconfigurable, intelligent, and sustainable wireless environments for 6G smart connectivity," *IEEE Commun. Mag.*, vol. 59, no. 10, pp. 99–105, Oct. 2021.

[13] W. Tang *et al*., "MIMO transmission through reconfigurable intelligent surface: System design, analysis, and implementation," *IEEE J. Sel. Areas Commun*, vol. 38, no. 11, pp. 2683–2699, Nov. 2020.

[14] W. Tang *et al*., "Realization of reconfigurable intelligent surface-based Alamouti space–time transmission," in *Proc. IEEE WCSP*, Nanjing, China, Oct. 2020, pp. 904–909.

[15] Y. Yang, B. Zheng, S. Zhang, and R. Zhang, "Intelligent reflecting surface meets OFDM: Protocol design and rate maximization," *IEEE Trans. Commun.*, vol. 68, no. 7, pp. 4522–4535, Jul. 2020.

[16] B. Zheng and R. Zhang, "Intelligent reflecting surface-enhanced OFDM: Channel estimation and reflection optimization," *IEEE Wireless Commun. Lett.*, vol. 9, no. 4, pp. 518–522, Apr. 2020.

[17] S. Lin *et al*., "Adaptive transmission for reconfigurable intelligent surface-assisted OFDM wireless communications," *IEEE J. Sel. Areas Commun.*, vol. 38, no. 11, pp. 2653–2665, Nov. 2020.

[18] G. C. Alexandropoulos, P. T. Mathiopoulos, and N. C. Sagias, "Switch-and-examine diversity over arbitrary correlated Nakagami-m fading channels," *IEEE Trans. Veh. Technol.*, vol. 59, no. 4, pp. 2080–2087, May 2010.

[19] G. C. Alexandropoulos, N. C. Sagias, F. I. Lazarakis, and K. Berberidis, "New results for the multivariate Nakagami-m fading model with arbitrary correlation matrix and applications," *IEEE Trans. Wireless Commun.*, vol. 8, no. 1, pp. 245–255, Jan. 2009.

[20] D. C. Chu, "Polyphase codes with good periodic correlation properties," *IEEE Trans. Inf. Theory*, vol. IT-18, no. 4, pp. 531–532, Jul. 1972.